Materials Science and Engineering C 69 (2016) 447–452

Contents lists available at ScienceDirect

Materials Science and Engineering C

journal homepage: www.elsevier.com/locate/msec

Porous graphene oxide nanostructure as an excellent scaffold for label-free electrochemical biosensor: Detection of cardiac troponin I

Sayed Habib Kazemi [a,*], Elham Ghodsi [b], Siamak Abdollahi [a], Samad Nadri [b,c,**]

[a] Department of Chemistry, Institute for Advanced Studies in Basic Sciences (IASBS), Zanjan 45137-66731, Iran
[b] Department of Medical Biotechnology and Nanotechnology, School of Medicine, Zanjan University of Medical Science, Zanjan, P.O. Box: 14115-111, Iran
[c] Cancer Gene Therapy Research Center, Zanjan University of Medical Science, Zanjan, Iran

ARTICLE INFO

Article history:
Received 17 April 2016
Received in revised form 30 June 2016
Accepted 4 July 2016
Available online 05 July 2016

Keywords:
Immunosensor
Porous graphene oxide
Glassy carbon electrode
Nanostructure
Electrochemical impedance
Cardiac troponin-I (cTnI)

ABSTRACT

Herein, we report the fabrication of a novel label-free impedimetric biosensor employing porous graphene oxide (PrGO) nanostructures for the specific detection of cardiac troponin-I (cTnI) to establish the myocardial infarction (MI). This nano-immunosensor demonstrates an outstanding selectivity and high sensitivity towards the human-cTnI analyte. An excellent detection limit of 0.07 ng mL^{-1} and dynamic linear range of 0.1–10 ng mL^{-1} were calculated for anti-cTnI/PrGO/GC. Finally, this biosensor was employed to check the concentration of the MI biomarker in real clinical samples and the results are in good agreement with standard enzyme-linked fluorescence assay (ELFA) method.

1. Introduction

During the last decades, carbon nanostructures including carbon nanotubes, carbon nanofibers, carbon mesostructures and graphene have shown great potential for application in electrochemical sensor and biosensors [1–4]. Recently, studies have shifted towards the electrochemical properties of graphene-based nanostructures, because of its superior electrochemical and electrical behavior in addition to its large active surface area. Thus, design and application of graphene based sensor and biosensors have attracted a great attention [5,6].

Acute myocardial infarction (AMI), the medical name for a heart attack, refers to a heart condition that is caused when the blood circulation or flow abruptly stops from the heart. This circulation break is always life-threatening situation and it may last long enough to cause tissue damage or death. Today, AMI is responsible for the highest rate of morbidity and mortality and one-third of deaths in the world occur because of this problem [7]. A timely and accurate diagnosis of AMI may accelerate treatment procedure; hence it will be beneficial to reduce the mortality rate. Determination the concentration of biomarkers in the blood sample is a critical factors to establish the AMI happening [8].

There are several biomarkers for the detection of cardiac infarction including C-reactive protein (CRP), cardiac troponin I, cardiac troponin T, myoglobin, lipoprotein-associated phospholipase, interlukin-6 and interlukin-1 (IL-6 and IL-1), and myeloperoxidase (MPO) in addition to tumor necrosis factor alpha (TNF-α) [9–16]. Amongst these biomarkers, determination of cTnI is preferred to diagnosis of AMI due to its excellent specificity and great sensitivity for acute myocardial cell damage [12,17,18]. It is worth mentioning that the normal value of cTnI in healthy human is about 0.4 ng mL^{-1} [19].

Currently, several methods are employed for cTnI analysis including conventional enzyme-linked immunosorbent assay (ELISA), Enzyme-linked Fluorescent Assay (ELFA) and radioimmunoassay (RIA) [20–23]. Most of these methods needs to be conducted under multistep processing of samples, long diagnostics times, and high cost [24]. Thus, a sensitive and facile method is required to perform the fast and accurate diagnosis of AMI.

During the last decades, several biosensors have been developed for analysis of cTnI including electrochemiluminescence, fluorescence, colorimetric, Surface plasmon resonance (SPR), Acoustic and cationic isotachophoresis [25–28]. However, most of these methods are based on labeling technology which is costly and time consuming procedure in addition to the complexity of the sensor fabrication.

Label free electrochemical biosensors can be considered as sustainable and inexpensive alternatives for biomarker analysis, in addition

* Corresponding author.
** Correspondence to: S. Nadri, Department of Medical Biotechnology and Nanotechnology, School of Medicine, Zanjan University of Medical Science, Zanjan, 14115-111, Iran.
E-mail addresses: habibkazemi@iasbs.ac.ir (S.H. Kazemi), nadrisamad@zums.ac.ir (S. Nadri).

http://dx.doi.org/10.1016/j.msec.2016.07.005
0928-4931/

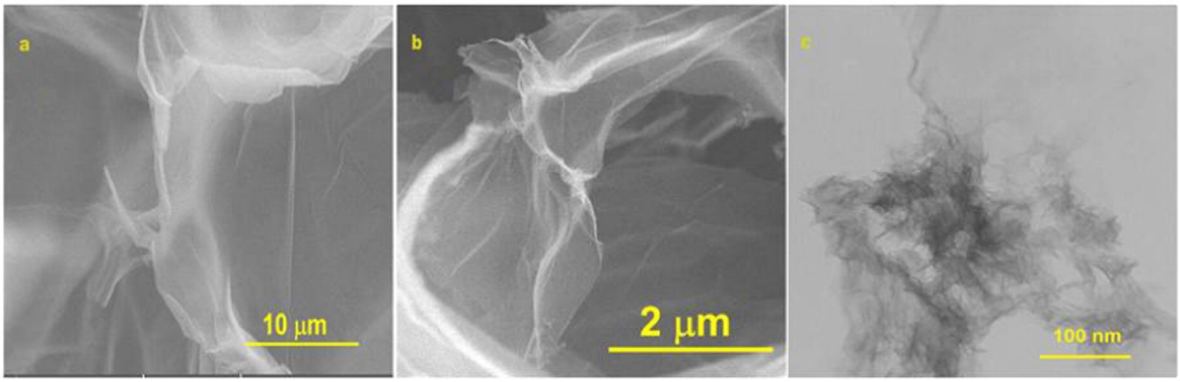

Fig. 1. (a) and (b) are the SEM micrographs of GO and PrGO, respectively. Also, (c) is a TEM image of PrGO nanostructures representing the porous structure of graphene sheets.

to their relatively short response time compared to other biosensors for cTnI detection [29].

Electrochemical based sensors and biosensors offered high sensitivity, considerable selectivity and low cost towards determination of chemical and biological species in the real samples [30–35]. Electrochemical methods, especially electrochemical impedance spectroscopy (EIS), are powerful techniques to monitor the events occurring on the electrode–electrolyte interfaces [6,30,31,34,36,37]. Thus, EIS has played a momentous role in the characterization of many types of biosensors for analyzing the species. Additionally, this method has a great potential to be used for label-free detection purposes [38–42].

In the present study, we introduce a novel and facile label-free electrochemical biosensor with ability of detecting the cTnI as AMI biomarker in patients. Herein, porous graphene oxide (PrGO), which is partially reduced, was employed as an excellent substrate to immobilize the anticardiac troponin-I (anti-cTnI) using the amide covalent bonding procedure. Our results indicate that the anti-cTnI/PGO biosensor can successfully detect the cTnI levels in a wide linear range of 0.1 to 10 ng mL^{-1}, with an excellent detection limit of 0.07 ng mL^{-1}.

2. Experimental and methods

2.1. Materials and instrumentations

Human cardiac troponin-I (cTnI) was purchased from R&D System and mouse anticardiac troponin-I (anti-cTnI) monoclonal (1E7) as an antibody was bought from Abcam. All other reagents were purchased from Sigma-Aldrich and used as received without further purification. All solutions were prepared with doubly distilled water. The electrochemical impedance spectroscopy (EIS) measurements were performed using a Zahner/Zennium potentiostat–galvanostat (Zahner, Germany). AC perturbation amplitude voltage of 10 mV was imposed on the open-circuit potential in the frequency range of 100 kHz to 100 mHz. EIS results were fitted to appropriate equivalent circuit based on the complex non-linear least square (CNLS) fitting procedure. The electrochemical experiments were carried out in a three electrode cell using a glassy carbon coated with porous graphene oxide and then modified with human cardiac troponin I as working electrode. Also, a platinum wire and an Ag/AgCl sat'd KCl were used as counter and reference electrodes, respectively. The structural characterization of porous graphene oxide was done by Fourier transform infrared (FTIR) spectroscopy using Vector 22 Bruker instrument, scanning electron microscopy (SEM, TESCAN VEGA3), transmission electron microscopy (TEM, Hitachi 200 kV electron beam energy) and atomic force microscopy (AFM, Nanoscope multimode atomic force microscope AFM, Ara, Iran).

Graphene oxide (GO) was synthesized from graphite flake using modified Hummer's method and finally converted to porous graphene oxide (PrGO) using freeze drying method.

To fabricate the biosensor, the glassy carbon electrode (GCE, a 2 mm diameter disk electrode purchased form CH instrument) was polished to have a mirror like finish. 3 mL of PrGO in dimethyl formamide (DMF) was placed on GCE and incubated for 1 h at 80 °C. Then, 5 μg mL^{-1} of anti-cTnI antibody was suspended in a solution of 0.1 M PBS (pH 7.4) containing 0.25 mg of sulfo-NHS and 0.5 mg of EDC and the PrGO/GCE was immersed in this solution at room temperature for 3 h. After that, the cTnI/PrGO/GCE was washed with PBS buffer to eliminate the nonspecific binding conjugates.

Different concentrations of human-cTnI were tested by cTnI/PrGO/GCE biosensor for 1 h. Then, the electrode was washed with PBS buffer to eliminate the nonspecific adsorbed species. Also, the effects of two major interferences (serum albumin and myoglobin) were studied. All experiments were performed in the presence of 5 mM of $K_3Fe(CN)_6$ and $K_4Fe(CN)_6$ as electro-active probe. Also, Enzyme-linked Fluorescent Assay (ELFA) of Troponin-I was employed as standard medical

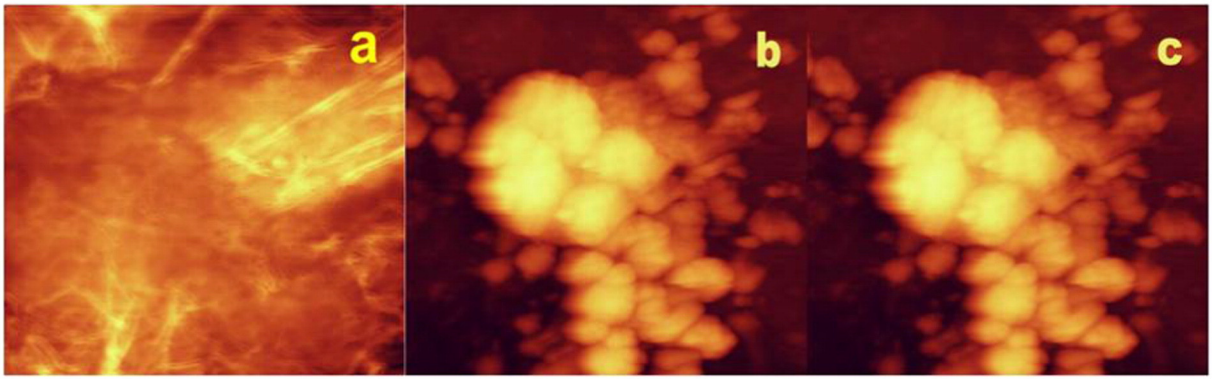

Fig. 2. AFM images (100 nm × 100 nm area) of (a) PrGO/GCE, (b) anti-cTnI/PrGO/GCE, and (c) anti-cTnI/PrGO/GCE incubated by human-cTnI proteins.

laboratory method to check the validity of the anti-cTnI/PrGO/GCE biosensor by a VIDAS instrument (BioMérieux, France).

3. Results and discussion

3.1. Characterization of GO, PrGO, and cTnI/PrGO electrodes

The morphology and structure of GO and PrGO nanosheets were investigated using SEM. Fig. 1a and b represent the SEM images of GO and PrGO nanosheets, respectively. As shown in Fig. 1b, nanosheets of porous graphene oxide are apart from each other and punched. High space and considerable porosity of PrGO nanosheets results in the large surface to volume ratio and increases the immobilization efficiency for cTnI in this work. Porous structure of graphene sheets was also confirmed by transmission electron microscopy (TEM) method (Fig. 1c).

Fig. 2 shows AFM images of various modified electrodes prepared in the present work. The average thickness of PrGO layers obtained by AFM analysis is almost 5 nm which confirms the aggregation of few single graphene sheets. Additionally, the average thickness for anti-cTnI/PrGO modified electrode was measured between 7–10 nm. Fig. 2b and c clearly reveal that the surfaces covered by anti-cTnI antibodies and coupling of human-cTnI proteins and anti-cTnI are much rougher than PrGO surface due to the large size of these proteins compared to the thickness of graphene sheets. Also, detailed topographic analysis showed that the porosity and distance of PrGO nanosheets are increased at the edges. This suggests that major fraction of functional groups are immobilized at the edges of graphene nanosheets. Therefore, an accumulation of anti-cTnI antibodies and consequently the cTnI proteins are observed at the edge of the nanosheets.

Moreover, Fourier transform infrared spectroscopy (FT-IR), as a powerful technique, was employed to confirm the formation and existence of functional groups at the GO and PrGO nanostructures. Fig. 3 illustrates the FT-IR spectra recorded for PrGO, anti-cTnI/PrGO, and anti-cTnI/PrGO incubated by cTnI protein. The FT-IR spectra show peaks at 1620–1750 cm^{-1}, which can be assigned to C═O stretching vibrations, also two bands at 1396 and 3410 cm^{-1} were attributed to O—H vibration. Besides, the bands at 1620 and 1064 cm^{-1} were attributed to C═C and C—O vibrations, respectively. Thus, FT-IR data supports the covalent bonding between PrGO and anti-cTnI antibody, as well as the interaction between antibody and antigen.

3.2. Electrochemical studies of anti-cTnI/PrGO/GCE biosensor

The sequential modification of electrodes with PrGO, cTnI antibody, and target human-cTnI was investigated using cyclic voltammograms recorded between −0.4 and +0.8 V vs Ag/AgCl with a scan rate of 25 mV s^{-1} in a 0.1 M of PBS solution (pH 7.4) containing 5 mM of both $K_3Fe(CN)_6$ and $K_4Fe(CN)_6$. As shown in Fig. 4, curve a, a pair of peaks assigned to the reversible one-electron redox reaction of Fe(III)/Fe(II) at GC electrode can be observed. After modification of GC electrode with PrGO, the current slightly decreased compared to the curve of bare electrode (Fig. 4, curve b). After incubation of PrGO/GC electrode with anti-cTnI antibody, the peak currents were decreased due to the substantial blockage of the electrode surface by antibody molecules (Fig. 4, curve c). Subsequently, a significant drop in peak currents were noticed after immobilization of target human-cTnI protein on the surface of PrGO/GC electrode (Fig. 4, curve d), as a result of increasing the electron transfer resistance at the biosensor surface. Thus, it is concluded that the successful interaction between the anti-cTnI and target human-cTnI at the biosensor surface is occurred.

Considering the change in the electron transfer resistance (R_{ct}) observed in cyclic voltammetry, EIS method was employed to inspect

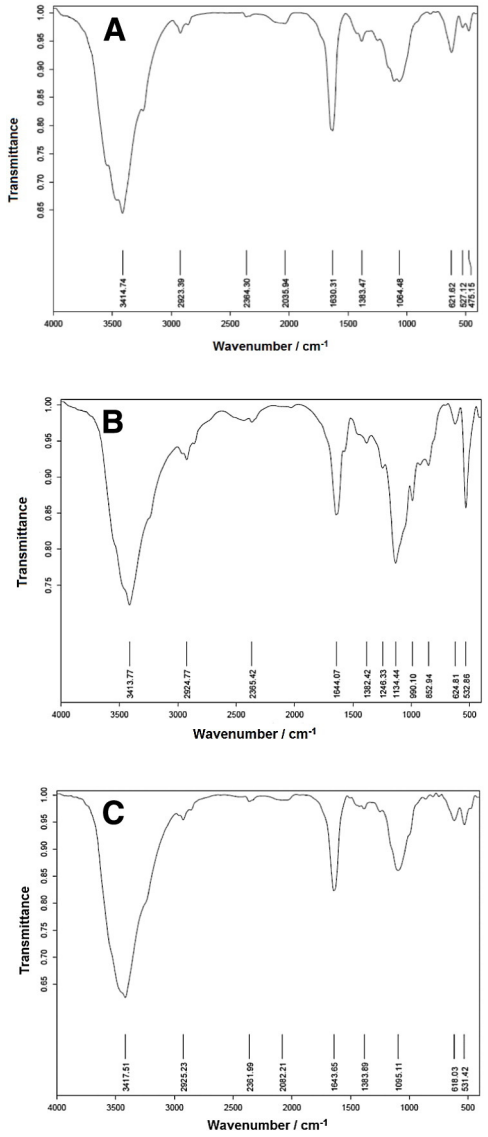

Fig. 3. FT-IR spectra recorded for (a) PrGO incubated by cTnI protein, (b) anti-cTnI/PrGO, and (c) anti-cTnI/PrGO incubated by cTnI protein.

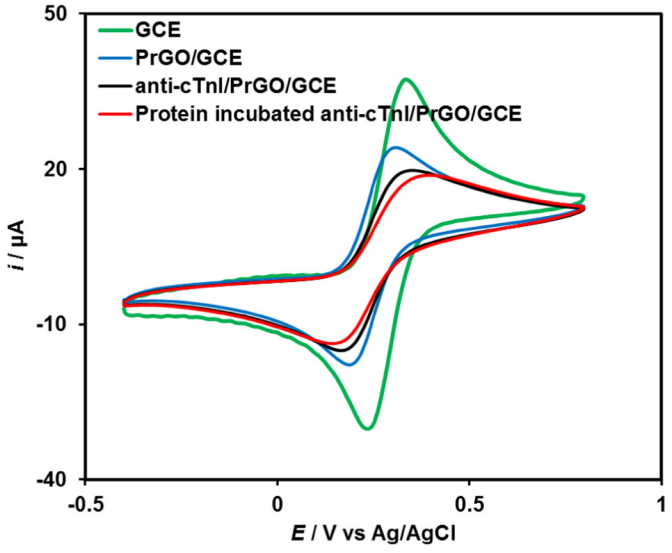

Fig. 4. Cyclic voltammograms recorded for (a) GCE, (b) PrGO/GCE, (c) anti-cTnI/PrGO/GC biosensor, and (d) anti-cTnI/PrGO/GC biosensor incubated with human-cTnI protein at a scan rate of 25 mV s^{-1} in a 0.1 M of PBS solution (pH 7.4) containing 5 mM of both $K_3Fe(CN)_6$ and $K_4Fe(CN)_6$.

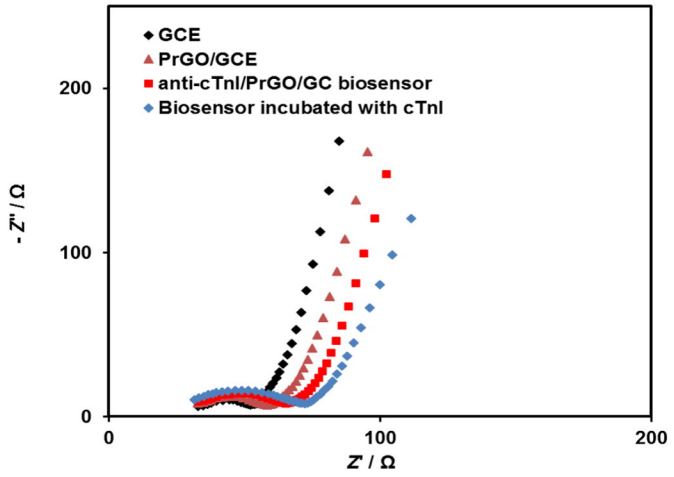

Fig. 5. Nyquist plots recorded for (a) GC, (b) PrGO/GC, (c) anti-cTnI/PrGO/GC, and (d) anti-cTnI/PrGO/GC biosensor incubated by cTnI protein at open-circuit potential.

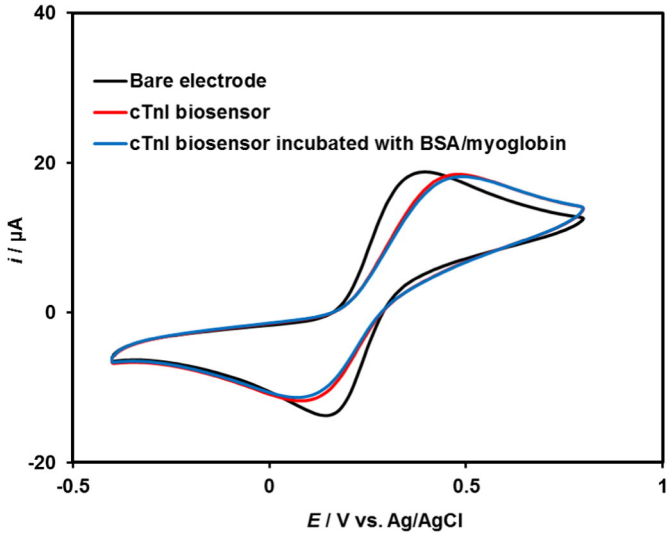

Fig. 6. Cyclic voltammograms recorded for PrGO/GC electrode (black), anti-cTnI/PrGO/GC biosensor (red), and anti-cTnI/PrGO/GC biosensor incubated with myoglobin and BSA proteins (both overlaid and represented in blue color) at a scan rate of 25 mV s^{-1} in a 0.1 M of PBS (pH 7.4) containing 5 mM of both $K_3Fe(CN)_6$ and $K_4Fe(CN)_6$. (For interpretation of the references to color in this figure legend, the reader is referred to the web version of this article.)

the precise relation of the interaction between antibody and target protein. The semicircle diameter in the Nyquist plot corresponds to the electron-transfer resistance (R_{ct}), which controls the electron-transfer kinetics of the redox probe at the biosensor interface. Fig. 5 represents the Nyquist plots for GCE, PrGO/GCE, anti-cTnI/PrGO/GCE, and anti-cTnI/PrGO/GCE incubated with human-cTnI protein. As seen, the charge-transfer resistance significantly increases by immobilization of anti-cTnI and after incubation of human-cTnI protein.

From Fig. 5c, it is observed that R_{ct} value increased after immobilization of anti-cTnI on the PrGO/GCE, indicating the decrease in the interfacial electron-transfer rate (estimated by complex nonlinear fitting method using ZMAN 2.0 software as 25 Ω). The amount of charge transfer resistance due to subsequent binding of the target protein and antibody, is also increased sharply (almost 42 from Fig. 5, curve d). Interestingly, the results of EIS experiments confirm the successful immobilization of anti-cTnI and human-cTnI.

To further quantify any background effect due to the nonspecific binding of non-conjugate target, anti-cTnI//PrGO/GC was fabricated and incubated with myoglobin and bovine serum albumin (BSA). Upon the addition of 60 ng mL^{-1} myoglobin protein and 40 ng/mL bovine serum albumin solutions to the anti-cTnI/PrGO/GC electrode, very small changes in the current was observed; providing an evidence for the absence of significant binding between myoglobin or BSA protein and anti-cTnI antibody (Fig. 6).

To further confirmation of the cyclic voltammetry results, similar tests were performed using EIS plots, with the anti-cTnI/PrGO/GC electrode incubated with myoglobin protein and BSA protein, showing insignificant change in the R_{ct} values (Fig. 7, curves b and c). These results indicate that insignificant affinity interaction is existed between anti-cTnI and myoglobin or BSA. Moreover, the applicability of the present biosensor was examined in several electrolytes including probable interfering ions at biological concentrations such as KCl, $CaCl_2$, NaCl, Na_2HPO_4, and mixed solutions of them. Insignificant changes were observed in the biosensor response in the absence of cTnI protein in different electrolytes. Also, the effect of the mentioned electrolytes on the biosensor signal for a fixed concentration of cTnI protein was inconsiderable. These observations confirmed the selectivity of the biosensor towards the human cTnI protein.

To examine the ability of anti-cTnI/PrGO/GCE to detect ultra-low concentrations of cTnI protein in biological samples, the effect of different concentrations of human-cTnI were analyzed by CV and EIS measurements.

Fig. 8a demonstrates the cyclic voltammograms recorded for anti-cTnI/PrGO/GC electrode in various concentrations of human-cTnI (0.1, 0.2, 0.5, 1.0, 2.0, 5.0, 7.0, and 10.0 ng mL^{-1}). By increasing the concentrations of human-cTnI, the current decreases compared to the curve of the anti-cTnI/PrGO/GC electrode in the absence of target protein. Fig. 8b shows the impedimetric responses of the biosensor for various concentrations of human-cTnI. As expected, the diameter of the appeared semicircle in Nyquist plots notably increased with increasing the concentration of human-cTnI. Using the impedance spectroscopy results, anti-cTnI/PrGO/GC biosensor responds linearly towards cTnI protein concentrations in the range of 0.1–10 ng mL^{-1} (each point was rechecked three times). Considering the standard deviation of the biosensor response to the blank sample, detection limit of the present biosensor was estimated as 0.07 ng mL^{-1}. The detection limit of the anti-cTnI/PrGO/GC biosensor is lower than much of the previously reported cTnI electrochemical biosensors. Thus, it can be concluded that the present study can show new horizons to develop and improve the facile and reliable electrochemical biosensors.

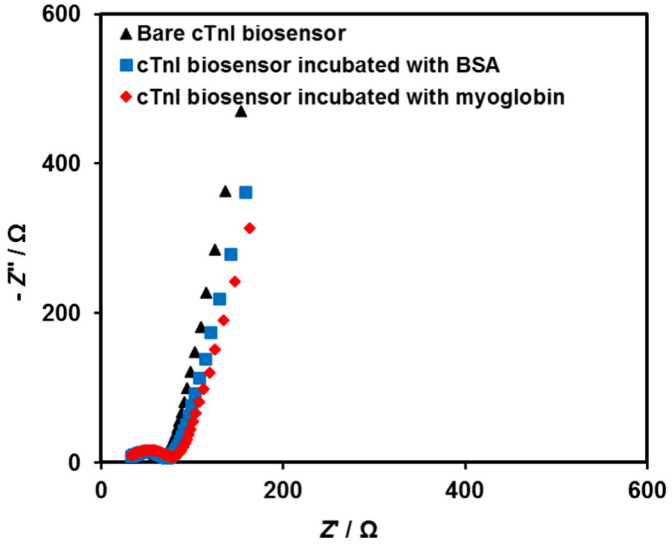

Fig. 7. Nyquist plots recorded for (a) bare anti-cTnI/PrGO/GCE, (b) anti-cTnI/PrGO/GCE incubated with myoglobin and (c) BSA proteins at open-circuit potential.

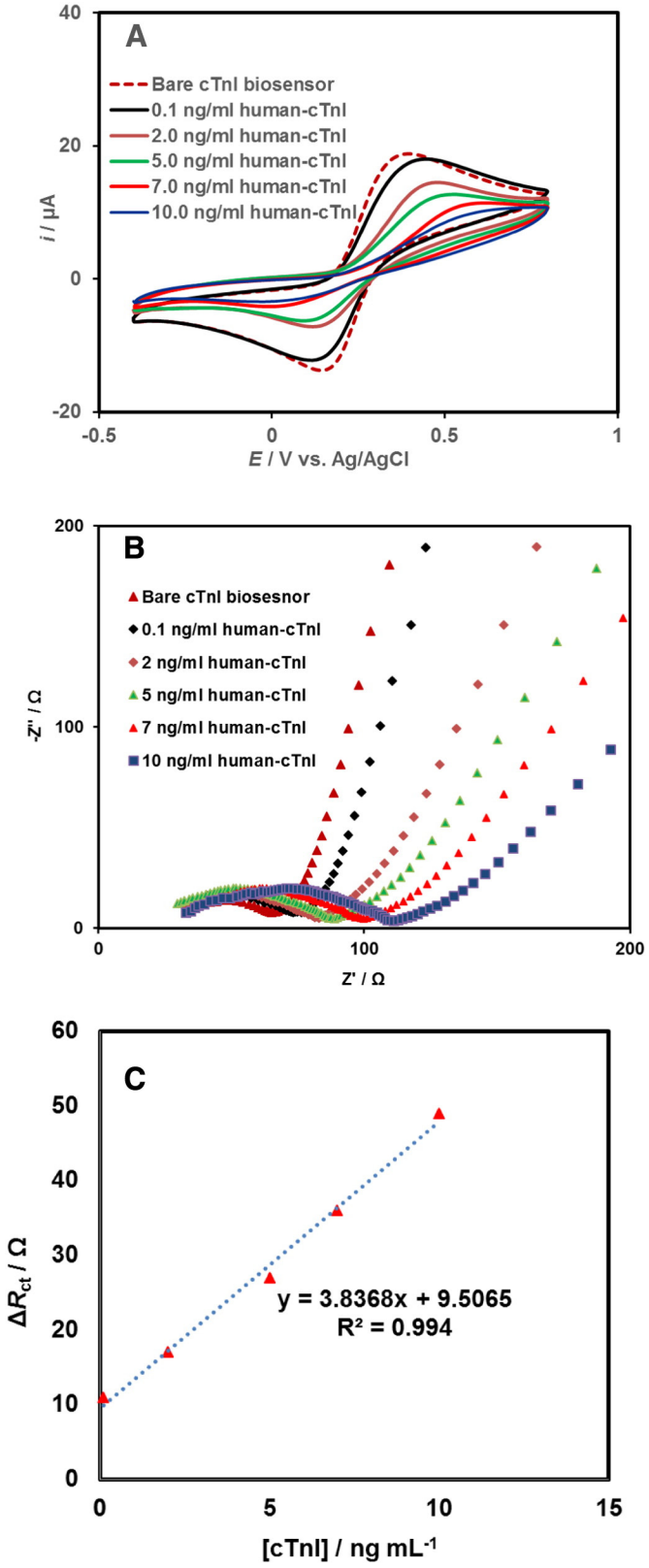

Fig. 8. (A) Cyclic voltammograms recorded for detection of various concentrations of human-cTnI at a scan rate of 25 mV s^{-1} in a 0.1 M of PBS solution (pH 7.4) in the presence of both $K_3Fe(CN)_6$ and $K_4Fe(CN)_6$ and (B) Nyquist diagrams of various concentrations of human-cTnI at open-circuit potential observed for anti-cTnI biosensor, and (C) plot of the biosensor response towards cTnI protein.

4. Conclusions

In the present work, porous graphene nanosheets was applied to design a novel label-free impedimetric biosensor for the selective detection of cardiac troponin-I protein as a biological marker to understand the myocardial infarction (MI). This nano-immunosensor demonstrates good selectivity and remarkable sensitivity towards the human-cTnI protein. Herein, an excellent detection limit of 0.07 ng mL^{-1} and relatively wide linear range of 0.1–10 ng mL^{-1} were calculated for anti-cTnI Ab/PrGO/GC. This biosensor was employed to check the concentration of the MI biomarker (human-cTnI protein) in real clinical samples and the results are in good agreement with standard ELFA method.

Acknowledgments

Financial supports of the work by Zanjan University of Medical Sciences and Institute for Advanced Studies in Basic Sciences (G2015IASBS32610) are appreciated.

References

[1] J.H. Jung, D.S. Cheon, F. Liu, K.B. Lee, T.S. Seo, Angew. Chem. Int. Ed. 49 (2010) 5708–5711.
[2] E. Rand, A. Periyakaruppan, Z. Tanaka, D.A. Zhang, M.P. Marsh, R.J. Andrews, K.H. Lee, B. Chen, M. Meyyappan, J.E. Koehne, Biosens. Bioelectron. 42 (2013) 434–438.
[3] A. Walcarius, Trends Anal. Chem. 38 (2012) 79–97.
[4] N. Yang, X. Chen, T. Ren, P. Zhang, D. Yang, Sensors Actuators B Chem. 207 (2015) 690–715.
[5] M. Pumera, Chem. Soc. Rev. 39 (2010) 4146–4157.
[6] S. Sabury, S.H. Kazemi, F. Sharif, Mater. Sci. Eng. C 49 (2015) 297–304.
[7] H.D. White, D.P. Chew, Lancet 372 (2008) 570–584.
[8] M.J. Lipinski, R.O. Escárcega, F. D'Ascenzo, M.A. Magalhães, N.C. Baker, R. Torguson, F. Chen, S.E. Epstein, Ò. Miró, P. Llorens, E. Giannitsis, U. Lotze, S. Lefebvre, M. Sebbane, J.-P. Cristol, C. Chenevier-Gobeaux, C. Meune, K.M. Eggers, S. Charpentier, R. Twerenbold, C. Mueller, G. Biondi-Zoccai, R. Waksman, Am. J. Cardiol. 113 (2014) 1581–1591.
[9] F.S. Apple, R.H. Christenson, R. Valdes, A.J. Andriak, A. Berg, S.-H. Duh, Y.-J. Feng, S.A. Jortani, N.A. Johnson, B. Koplen, K. Mascotti, A.H.B. Wu, Clin. Chem. 45 (1999) 199–205.
[10] S. Baldus, C. Heeschen, T. Meinertz, A.M. Zeiher, J.P. Eiserich, T. Münzel, M.L. Simoons, C.W. Hamm, O.B.O.T.C. Investigators, Circulation 108 (2003) 1440–1445.
[11] M.J. Caslake, C.J. Packard, K.E. Suckling, S.D. Holmes, P. Chamberlain, C.H. Macphee, Atherosclerosis 150 (2000) 413–419.
[12] B. Cummins, P. Cummins, J. Mol. Cell. Cardiol. 19 (1987) 999–1010.
[13] H.A. Katus, A. Remppis, T. Scheffold, K.W. Diederich, W. Kuebler, Am. J. Cardiol. 67 (1991) 1360–1367.
[14] P. Kui, L.W.G. Chunrui, Clin. Cardiol. 3 (1999) 009.
[15] P.M. Ridker, R.J. Glynn, C.H. Hennekens, Circulation 97 (1998) 2007–2011.
[16] P.M. Ridker, N. Rifai, M. Pfeffer, F. Sacks, S. Lepage, E. Braunwald, f.t. cholesterol, R.E. investigators, Circulation 101 (2000) 2149–2153.
[17] G.S. Bodor, S. Porter, Y. Landt, J.H. Ladenson, Clin. Chem. 38 (1992) 2203–2214.
[18] B. Cummins, M.L. Auckland, P. Cummins, Am. Heart J. 113 (1987) 1333–1344.
[19] E.M. Antman, M.J. Tanasijevic, B. Thompson, M. Schactman, C.H. McCabe, C.P. Cannon, G.A. Fischer, A.Y. Fung, C. Thompson, D. Wybenga, E. Braunwald, N. Engl. J. Med. 335 (1996) 1342–1349.
[20] F.S. Apple, A. Falahati, P.R. Paulsen, E.A. Miller, S.W. Sharkey, Clin. Chem. 43 (1997) 2047–2051.
[21] D. Bader, T. Masaki, D.A. Fischman, J. Cell Biol. 95 (1982) 763–770.
[22] S.-S. Chang, S.-H. Lee, J.-Y. Wu, H.-C. Ning, T.-F. Chiu, F.-L. Wang, J.H. Chen, C.-H. Li, C.-C. Lee, R.-C. Chan, J. Thromb. Thrombolysis 30 (2010) 472–478.
[23] J. Wang, A. Ibáñez, M.P. Chatrathi, A. Escarpa, Anal. Chem. 73 (2001) 5323–5327.
[24] Z. Yang, D. Min Zhou, Clin. Biochem. 39 (2006) 771–780.
[25] D. Bottenus, T.Z. Jubery, Y. Ouyang, W.-J. Dong, P. Dutta, C.F. Ivory, Lab Chip 11 (2011) 890–898.
[26] P. Nandhikonda, M.D. Heagy, J. Am. Chem. Soc. 133 (2011) 14972–14974.
[27] W. Shen, D. Tian, H. Cui, D. Yang, Z. Bian, Biosens. Bioelectron. 27 (2011) 18–24.
[28] W.-Y. Wu, Z.-P. Bian, W. Wang, W. Wang, J.-J. Zhu, Sensors Actuators B Chem. 147 (2010) 298–303.
[29] X. Luo, J.J. Davis, Chem. Soc. Rev. 42 (2013) 5944–5962.
[30] H. Beitollahi, H. Karimi-Maleh, H. Khabazzadeh, Anal. Chem. 80 (2008) 9848–9851.
[31] H. Beitollahi, M. Mostafavi, Electroanalysis 26 (2014) 1090–1098.
[32] S.H. Kazemi, B. Hosseinzadeh, S. Zakavi, Sensors Actuators B Chem. 210 (2015) 343–348.
[33] S.H. Kazemi, R. Mohamadi, Electrochim. Acta 109 (2013) 823–827.
[34] H. Beitollahi, M.M. Ardakani, B. Ganjipour, H. Naeimi, Biosens. Bioelectron. 24 (2008) 362–368.
[35] E. Molaakbari, A. Mostafavi, H. Beitollahi, R. Alizadeh, Analyst 139 (2014) 4356–4364.
[36] S.H. Kazemi, A. Alizadeh, R. Mohamadi, M.M. Khodaei, D. Kordestani, Mater. Sci. Eng. C 33 (2013) 5095–5099.

[37] S.H. Kazemi, M. Shanehsaz, M. Ghaemmaghami, Mater. Sci. Eng. C 52 (2015) 151–154.
[38] S.H. Kazemi, M. Shamsipur, A. Alizadeh, M.F. Mousavi, J. Iran. Chem. Soc. 10 (2012) 333–338.
[39] A.-E. Radi, J.L. Acero Sánchez, E. Baldrich, C.K. O'Sullivan, Anal. Chem. 77 (2005) 6320–6323.
[40] M. Shamsipur, S.H. Kazemi, A. Alizadeh, M.F. Mousavi, M.S. Workentin, J. Electroanal. Chem. 610 (2007) 218–226.
[41] M. Shamsipur, S.H. Kazemi, A. Mehdinia, M.F. Mousavi, H. Sharghi, Electroanalysis 20 (2008) 513–519.
[42] H. Xu, K. Gorgy, C. Gondran, A. Le Goff, N. Spinelli, C. Lopez, E. Defrancq, S. Cosnier, Biosens. Bioelectron. 41 (2013) 90–95.